ÉCOLE POLYTECHNIQUE FÉDÉRALE DE LAUSANNE

MATHICSE

Mathematics Institute of Computational Science and Engineering

School of Basic Sciences - Section of Mathematics

MATHICSE Technical Report

Nr. 19 .2016

June 2016

Automatic reduction of PDEs defined on domains with variable shape

Andrea Manzoni, Federico Negri

http://mathicse.epfl.ch

Address: EPFL - SB - MATHICSE (Bâtiment MA)
Station 8 - CH-1015 - Lausanne - Switzerland

Phone: +41 21 69 37648

Automatic reduction of PDEs defined on domains with variable shape

Andrea Manzoni and Federico Negri

Abstract In this work we propose a new, general and computationally cheap way to tackle parametrized PDEs defined on domains with variable shape when relying on the reduced basis method. We easily describe a domain by boundary parametrizations, and obtain domain deformations by solving a solid extension through a linear elasticity problem. The procedure is built over a two-stages reduction: *(i)* first, we construct a reduced basis approximation for the mesh motion problem; *(ii)* then, we generate a reduced basis approximation of the state problem, relying on finite element snapshots evaluated over a set of reduced deformed configurations. A Galerkin-POD method is employed to construct both the reduced problems, although this choice is not restrictive. To deal with unavoidable non affinities arising in both cases, we apply a matrix version of the discrete empirical interpolation method, allowing to treat geometrical deformations in a non-intrusive, efficient and purely algebraic way. In order to assess the numerical performances of the proposed technique we consider the solution of a parametrized (direct) Helmholtz scattering problem where the parameters describe both the shape of the obstacle and other relevant physical features.

1 Introduction

The reduced basis (RB) method provides nowadays a very efficient approach for the numerical approximation of problems arising e.g. from engineering and applied sciences which require the repeated solution of differential equations. Well-known instances include partial differential equations (PDEs) depending on several parameters, PDE-constrained optimization, as well as optimal control and design problems.

A. Manzoni · F. Negri
CMCS-MATHICSE-SB, Ecole Polytechnique Fédérale de Lausanne,
Station 8, CH-1015 Lausanne, Switzerland
e-mail: andrea.manzoni@epfl.ch, federico.negri@epfl.ch

In all these cases, the RB method replaces the original large-scale numerical problem (or high-fidelity approximation) originated by applying, e.g., a finite element (FE) method, with a reduced problem of substantially smaller dimension [25, 14].

In all these contexts, relevant instances of parametrized PDEs arise when dealing with problems defined over spatial domains undergoing geometrical transformations; this is the case of design problems, where being able to rapidly adapt existing meshes to design variations is essential to perform, e.g., shape optimization in an efficient way.

On the other hand, an offline/online stratagem, relying on the so-called *affine parametric dependence*, is required to gain a strong computational speedup when dealing with RB approximations to parametrized PDEs. In this respect, dealing with shape variations has often a major impact on the computational efficiency, since:

1. equipping the set of varying shape with a suitable *parametrization* is an involved, highly problem-dependent, task. In the RB context, parametric maps defined over the whole domain are needed to formulate the PDE problem on a parameter-independent reference configuration. However, in computed-aided design (CAD), *boundary parametrizations* under analytic form are usually defined for surfaces (in $d = 3$ dimensions) or curves ($d = 2$), rather than for the whole domain, thus preventing their direct use within the RB context;
2. geometrical parametrizations usually yield nonaffine parametric dependencies, so that an affine approximation of PDE operators has to be recovered through the *empirical interpolation method* (EIM) [3, 19] – or its discrete counterpart (DEIM) [6]. This usually entails an extensive work on the continuous formulation of the problem, as well as intrusive changes to its high-fidelity implementation.

Several techniques have been exploited to perform RB approximations of PDEs defined on varying domains. The simplest idea is to rely on *affine maps*, which automatically induce an affine parametric dependence, but only enable elementary deformations [26].

More involved deformations can be obtained by introducing *nonaffine maps* yielding *volume-based parametrizations*. Within this class, we mention *free-form deformations* (FFD) [18, 27, 21, 2] and interpolation relying on *radial basis functions* (RBF) [20, 23, 8, 10] as remarkable instances. Both techniques originate global deformations by combining the displacements of a set of control points. FFD deal with a cartesian lattice of control points and a tensor product of splines to combine control points displacements; these latter are instead interpolated in the RBF case, where the control points can be freely located inside the domain. In both cases, however, selecting the number of control points, their position and admissible displacements is far from being trivial.

Another option relies instead on the use of *transfinite mappings*, which define the interior points of the original domain as linear combinations of points on the boundaries [11]. In particular, each edge of the original domain is obtained as a one-to-one mapping of the corresponding edge on the reference domain, through a vector of geometrical parameters, see e.g. [9, 15, 16].

Finally, *isogeometric analysis* has been recently exploited in [22] as a possible way to deal with parametrized profiles with respect to parameters (such as the NACA number in the case of flows past airfoils) of simple interpretation.

The mesh motion strategy considered in this work allows to simplify the way to deal with geometrical deformations, by relying on *(i)* simple boundary parametrizations, and *(ii)* the solution of a solid extension problem. Moreover, we exploit a recently proposed matrix version of DEIM (MDEIM, [23, 35, 5]) to perform inexpensive evaluations of the online matrix operators for both the deformation and the state problem. Hence, we first recover an affine parametric dependence in the high-fidelity arrays appearing in both problems, by applying MDEIM and DEIM for matrix and vector operators, respectively. This is performed in a purely algebraic, black-box, in order to overcome the application of the EIM on the continuous formulation of the problem, which is usually highly demanding, see e.g. [12, 24, 4]. Then, we perform the RB approximation of both the deformation and the state problem, relying on a Galerkin-POD technique.

The paper is structured as follows. In Sect. 2 we describe the proposed mesh deformation technique. In Sect. 3 we introduce the class of problems we deal with in this work, as well as the main features of the RB approximation framework we develop. The whole computational procedure is then applied in Sect. 4 for the sake of the efficient solution of a parametrized (direct) Helmholtz scattering problem. Finally, some conclusions are reported in Sect. 5.

2 Solid extension mesh moving techniques

Let $\widetilde{\Omega} \subset \mathbb{R}^d$ be a spatial domain with boundary $\widetilde{\Gamma}$, where $d = 2,3$ is the number of space dimensions. We denote by $\widetilde{\Gamma}_h$ a discretization of the boundary $\widetilde{\Gamma}$ and by $\widetilde{\Omega}_h$ a volumetric mesh of that geometry, e.g. a triangular mesh in 2D or a tetrahedral mesh in 3D. Given a boundary deformation $\widetilde{\Gamma}_h \mapsto \Gamma_h$, mesh deformation techniques adapt the mesh $\widetilde{\Omega}_h$ such that *(i)* the updated mesh Ω_h conforms to the updated boundary, i.e. $\partial\Omega_h = \Gamma_h$ and *(ii)* the geometric embedding of Ω_h (i.e., its nodes positions) is modified while keeping fixed the mesh topology (i.e., its connectivity).

Among a wide range of existing mesh deformation techniques, here we focus on the so called *mesh-based variational methods* (see, e.g., [30]). These latter compute smooth harmonic [1], biharmonic [13] or elastic [33, 32, 31] deformations by solving Laplacian, bi-Laplacian or elasticity problems, respectively. Specifically, we consider this latter, which is often referred to as solid-extension mesh moving technique (SEMMT) [33, 32, 31].

Before describing the method, let us first introduce a non-overlapping decomposition of the boundary Γ into a deformable portion $\widetilde{\gamma}$ and a fixed one $\partial\Omega \setminus \widetilde{\gamma}$. Given a boundary displacement $\boldsymbol{h} \in [H^{1/2}(\widetilde{\gamma})]^d$ such that $\gamma = \{\mathbf{x} \in \mathbb{R}^d \ : \ \mathbf{x} = \tilde{\mathbf{x}} + \boldsymbol{h},\ \tilde{\mathbf{x}} \in \widetilde{\Omega}\}$, the SEMMT generates a deformed domain Ω as

$$\Omega(\boldsymbol{h}) = \{\mathbf{x} \in \mathbb{R}^d \ : \ \mathbf{x} = \tilde{\mathbf{x}} + \boldsymbol{d}(\boldsymbol{h}),\ \tilde{\mathbf{x}} \in \widetilde{\Omega}\}$$

where $\boldsymbol{d} = \boldsymbol{d}(\boldsymbol{h}) \in [H^1(\widetilde{\Omega})]^d$ is the displacement field solution of the following linear elasticity problem:

$$\begin{cases} -\operatorname{div}(\boldsymbol{\sigma}(\boldsymbol{d})) = \boldsymbol{0} & \text{in } \widetilde{\Omega} \\ \boldsymbol{d} = \boldsymbol{h} & \text{on } \widetilde{\gamma} \\ \boldsymbol{d} = \boldsymbol{0} & \text{on } \partial\widetilde{\Omega} \setminus \widetilde{\gamma}. \end{cases} \tag{1}$$

Here, $\boldsymbol{\sigma}(\boldsymbol{d}) = 2\mu\boldsymbol{\varepsilon}(\boldsymbol{u}) + \lambda \operatorname{div}(\boldsymbol{d})\boldsymbol{I}$ is the Cauchy stress tensor , λ and μ are the Lamé constants, $\boldsymbol{I}$ is the identity tensor and $\boldsymbol{\varepsilon}(\boldsymbol{d}) = \frac{1}{2}(\nabla\boldsymbol{d} + \nabla\boldsymbol{d}^T)$ is the strain tensor.

Since the SEMMT is then applied at the discrete level, we introduce the FE trial and test functions spaces

$$V_h(\boldsymbol{h}) = \{\boldsymbol{v}_h \,|\, \boldsymbol{v}_h \in [P_h]^d,\ \boldsymbol{v}_h|_{\widetilde{\gamma}_h} = \boldsymbol{h},\ \boldsymbol{v}_h|_{\partial\widetilde{\Omega}_h \setminus \widetilde{\gamma}_h} = \boldsymbol{0}\},$$

$$V_h^0 = \{\boldsymbol{v}_h \,|\, \boldsymbol{v}_h \in [P_h]^d,\ \boldsymbol{v}_h|_{\partial\widetilde{\Omega}} = \boldsymbol{0}\},$$

where P_h denotes a FE space made of piecewise polynomial nodal basis functions. The high-fidelity FE approximation of (1) reads as follows: find $\boldsymbol{d}_h \in V_h(\boldsymbol{h})$ such that

$$\int_{\widetilde{\Omega}_h} \boldsymbol{\sigma}(\boldsymbol{d}_h) : \boldsymbol{\varepsilon}(\boldsymbol{v}_h)\, d\widetilde{\Omega} = 0 \qquad \forall \boldsymbol{v}_h \in V_h^0. \tag{2}$$

As described in [32], the method is then augmented with a proper Jacobian-based stiffening in order to enhance the mesh quality. To this end, the way we account for the Jacobian of the transformation from the element domain to the physical domain is altered by replacing the global integrals in (2) as follows

$$\int_{\widetilde{\Omega}_h} [\cdots]\, d\widetilde{\Omega} = \sum_{e \in \widetilde{\Omega}_h} \int_{\Xi} [\cdots]^e J^e\, d\Xi \quad \longrightarrow \quad \sum_{e \in \widetilde{\Omega}_h} \int_{\Xi} [\cdots]^e J^e \left(\frac{J^0}{J^e}\right)^{\eta} d\Xi. \tag{3}$$

Here, Ξ denotes the reference element, J^e is the Jacobian of the element e, J^0 is an arbitrary scaling parameter and $\eta \in \mathbb{R}_+$ is the so-called stiffening power.

At the algebraic level, problem (2) yields a linear system of large dimension $N_h^d \times N_h^d$ to be solved,

$$\mathbb{B}(\eta)\mathbf{d}_h = \mathbf{g}(\boldsymbol{h}), \tag{4}$$

where $\mathbf{d}_h \in \mathbb{R}^{N_h^d}$, $\mathbb{B}(\eta) \in \mathbb{R}^{N_h^d \times N_h^d}$ and the right-hand side vector $\mathbf{g}(\boldsymbol{h}) \in \mathbb{R}^{N_h^d}$ encodes the action of the nonhomogeneous Dirichlet condition imposed on $\widetilde{\gamma}$.
Given a boundary displacement $\boldsymbol{h}$, solving (4) thus allows to obtain a deformed volumetric mesh

$$\Omega_h(\boldsymbol{h}) = \{\mathbf{x}_h \in \mathbb{R}^d \ :\ \mathbf{x}_h = \tilde{\mathbf{x}}_h + \mathbf{d}_h(\eta, \boldsymbol{h}),\ \tilde{\mathbf{x}}_h \in \widetilde{\Omega}_h\}.$$

which satisfies the requirements *(i)* and *(ii)*.

The boundary displacement $\boldsymbol{h}$ can be generated in different ways depending on the application at hand. In this work, we consider the simplest case where $\boldsymbol{h}$ is given

in the form of a parameter-dependent analytic function. To make an example, let us consider the 2D domain $\Omega = D(\mathbf{0};5) \setminus D(\mathbf{0};1)$, where $D(\mathbf{x}_c;r)$ denotes the open disk of center $\mathbf{x}_c$ and radius r. A family of boundary deformations parametrized with respect to a vector of two parameters (α,β) could be defined as follows [7]

$$\boldsymbol{h} = [\cos(t) + \alpha\cos(2t) - \alpha,\ \beta\sin(t)] \tag{5}$$

with $t = \text{atan2}(\tilde{\mathbf{x}}_1, \tilde{\mathbf{x}}_2) \in [0, 2\pi]$, see Fig. 1. A more advanced alternative would be to use suitable boundary morphing techniques like RBF or the design element approach, see e.g. [36]. In all these cases, however, the boundary deformation is controlled through a (possibly small) set $\mathscr{P}_g \subset \mathbb{R}^g$ of geometrical parameters $\boldsymbol{\mu}_g$, i.e. $\boldsymbol{h} = \boldsymbol{h}(\boldsymbol{\mu}_g)$. For instance, in the case of expression (5) we have $\boldsymbol{\mu}_g = (\alpha,\beta,\eta)$, by considering the stiffening power $\eta \in \mathbb{R}_+$ as a further parameter. As a result, the *mesh motion (MM) problem* turns into the following parametrized problem: given $\boldsymbol{\mu}_g \in \mathscr{P}_g$, find the displacement field $\mathbf{d}_h \in \mathbb{R}^{N_h^d}$ such that

$$\mathbb{B}(\boldsymbol{\mu}_g)\mathbf{d}_h = \mathbf{g}(\boldsymbol{\mu}_g). \tag{6}$$

Note that the dependence of problem (6) on the parameters defining the family of boundary deformations is only through its right-hand side $\mathbf{g}$.

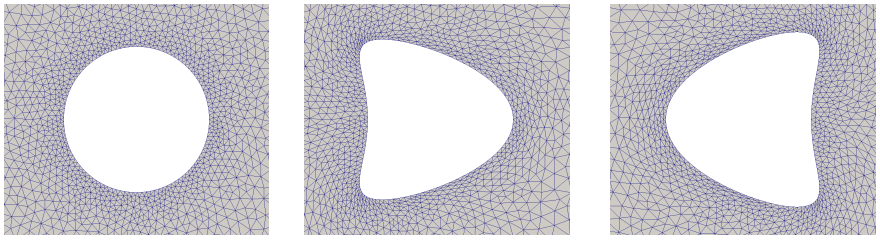

Fig. 1 Left: undeformed volumetric mesh $\widetilde{\Omega}_h$; center and right: examples of deformed volumetric meshes $\Omega_h(\boldsymbol{h})$ obtained through (5)

3 Reduced basis approximation: POD-Galerkin techniques and matrix DEIM

Solving problem (1) allows to compute a displacement field over the whole domain; any parameter-dependent instance of the domain thus result by applying the displacement to the reference, parameter-independent, domain $\widetilde{\Omega} \subset \mathbb{R}^d$, that is,

$$\Omega(\boldsymbol{\mu}_g) = \{\mathbf{x} \in \mathbb{R}^d \ :\ \mathbf{x} = \tilde{\mathbf{x}} + \mathbf{d}(\boldsymbol{\mu}_g),\ \tilde{\mathbf{x}} \in \widetilde{\Omega}\}, \quad \boldsymbol{\mu}_g \in \mathscr{P}_g;$$

the computational mesh $\widetilde{\Omega}_h$ over which the state problem is solved is then given by

$$\Omega_h(\boldsymbol{\mu}_g) = \{\mathbf{x}_h \in \mathbb{R}^d \ : \ \mathbf{x}_h = \tilde{\mathbf{x}}_h + \mathbf{d}_h(\boldsymbol{\mu}_g),\ \tilde{\mathbf{x}}_h \in \widetilde{\Omega}_h\}, \quad \boldsymbol{\mu}_g \in \mathscr{P}_g,$$

being $\mathbf{d}_h = \mathbf{d}_h(\boldsymbol{\mu}_g)$ the solution of the high-fidelity problem (6). Since its solution for any parameter vector $\boldsymbol{\mu}_g \in \mathscr{P}_g$ would be computationally expensive, we rather approximate the displacement field by relying on the RB method, whose main ingredients will be detailed in the following. Hence, we approximate $\mathbf{d}_h(\boldsymbol{\mu}_g) \approx \mathbb{V}\mathbf{d}_N(\boldsymbol{\mu}_g)$ as a linear combination of N_d (deformation) basis functions, being $\mathbf{d}_N \in \mathbb{R}^{N_d}$ a vector of coefficients. The latter is the solution of a problem obtained by projecting the high-fidelity system (6) onto the basis $\mathbb{V}$, as we shall describe later.

As a result, the set of parametrized domains we deal with is given by

$$\left\{\Omega_h^N(\boldsymbol{\mu}_g) = \{\mathbf{x}_h^N \in \mathbb{R}^d \ : \ \mathbf{x}_h^N = \tilde{\mathbf{x}}_h + \mathbb{V}\mathbf{d}_N(\boldsymbol{\mu}_g),\ \tilde{\mathbf{x}}_h \in \widetilde{\Omega}_h\}, \quad \boldsymbol{\mu}_g \in \mathscr{P}_g\right\}; \tag{7}$$

provided that the error $\|\mathbf{d}_h(\boldsymbol{\mu}_g) - \mathbb{V}\mathbf{d}_N(\boldsymbol{\mu}_g)\|$ is sufficiently small – this is indeed ensured by standard algorithms in the RB context – $\Omega_h^N(\boldsymbol{\mu}_g)$ yields an accurate approximation of $\Omega_h(\boldsymbol{\mu}_g)$.

3.1 Formulation of the state problem

Let us now move to the state problem we finally want to solve. For the sake of illustration, we consider as state problem the case of a scalar linear elliptic stationary PDE, although the proposed technique can be extended to more general problems in a straightforward way. Let us denote by $W = W(\boldsymbol{\mu}_g)$ a suitable Hilbert space, defined over the parameter-dependent domain $\Omega(\boldsymbol{\mu}_g) \subset \mathbb{R}^d$; in abstract form, the parametrized problem we focus on can be written as follows: given $\boldsymbol{\mu} = (\boldsymbol{\mu}_g, \boldsymbol{\mu}_p) \in \mathscr{P} = \mathscr{P}_g \times \mathscr{P}_p \subset \mathbb{R}^{g+p}$, find $u(\boldsymbol{\mu}) \in W(\boldsymbol{\mu}_g)$ such that

$$a(u(\boldsymbol{\mu}), v; \boldsymbol{d}(\boldsymbol{\mu}_g), \boldsymbol{\mu}_p) = f(v; \boldsymbol{d}(\boldsymbol{\mu}_g), \boldsymbol{\mu}_p) \qquad \forall v \in W(\boldsymbol{\mu}_g); \tag{8}$$

here $\boldsymbol{\mu}_p$ denotes a vector of physical parameters only affecting the state problem. Note that the presence of the displacement $\boldsymbol{d}(\boldsymbol{\mu}_g)$, playing the role of known parametrized field in (8), induces a dependence of both the bilinear form $a(\cdot,\cdot;\boldsymbol{d}(\boldsymbol{\mu}_g),\boldsymbol{\mu}_p)$: $W(\boldsymbol{\mu}_g) \times W(\boldsymbol{\mu}_g) \to \mathbb{C}$ and the linear form $f(\cdot;\boldsymbol{d}(\boldsymbol{\mu}_g),\boldsymbol{\mu}_p) : W(\boldsymbol{\mu}_g) \to \mathbb{C}$ on $\boldsymbol{\mu}_g$, too.

Here we assume that $a(\cdot,\cdot;\boldsymbol{d}(\boldsymbol{\mu}_g),\boldsymbol{\mu}_p)$ is continuous and weakly coercive over $W \times W$, and that $f(\cdot;\boldsymbol{d}(\boldsymbol{\mu}_g),\boldsymbol{\mu}_p)$ is continuous, for any $(\boldsymbol{\mu}_g,\boldsymbol{\mu}_p)$, so that problem (8) admits a unique solution thanks to Nečas theorem.

The high-fidelity, FE approximation of problem (8) can then be obtained upon defining a FE space $W_h(\boldsymbol{\mu}_g) \subset W(\boldsymbol{\mu}_g)$ over the domain $\Omega_h^N(\boldsymbol{\mu}_g)$, and seeking $u_h(\boldsymbol{\mu}) \in W_h(\boldsymbol{\mu}_g)$ such that

$$a(u_h(\boldsymbol{\mu}), v_h; \mathbf{d}_N(\boldsymbol{\mu}_g), \boldsymbol{\mu}_p) = f(v_h; \mathbf{d}_N(\boldsymbol{\mu}_g), \boldsymbol{\mu}_p) \qquad \forall v_h \in W_h(\boldsymbol{\mu}_g); \tag{9}$$

note that we have already considered the RB approximation of the displacement field. From an algebraic standpoint, problem (9) yields a linear system of large di-

mension $N_h^u \times N_h^u$ to be solved,

$$\mathbb{A}(\boldsymbol{\mu})\mathbf{u}_h(\boldsymbol{\mu}) = \mathbf{f}(\boldsymbol{\mu}), \tag{10}$$

where $\mathbb{A}(\boldsymbol{\mu}) = \mathbb{A}(\mathbf{d}_N(\boldsymbol{\mu}_g);\boldsymbol{\mu}_p) \in \mathbb{R}^{N_h^u \times N_h^u}$ and $\mathbf{f}(\boldsymbol{\mu}) = \mathbf{f}(\mathbf{d}_N(\boldsymbol{\mu}_g);\boldsymbol{\mu}_p) \in \mathbb{R}^{N_h^u}$.

3.2 POD-Galerkin reduced order models

Problems (6) and (10) share the same nature of parameter-dependent, high dimensional, linear systems arising from the discretization of two different second-order parametrized PDEs. To solve them efficiently, we rely in both cases on the RB method, thus approximating the unknowns $\mathbf{u}_h$ in a basis $\mathbb{W} \in \mathbb{R}^{N_h^u \times N_u}$, $\mathbf{d}_h$ in a basis $\mathbb{V} \in \mathbb{R}^{N_h^d \times N_d}$ of reduced dimensions $N_u \ll N_h^u$, $N_d \ll N_h^d$, i.e. $\mathbf{u}_h(\boldsymbol{\mu}) \approx \mathbb{W}\mathbf{u}_N(\boldsymbol{\mu})$, $\mathbf{d}_h(\boldsymbol{\mu}_g) \approx \mathbb{V}\mathbf{d}_N(\boldsymbol{\mu}_g)$. Then, we enforce the orthogonality of the residual of each equation to $\mathbb{W}$ and $\mathbb{V}$, respectively, thus resulting in two Galerkin-RB problems under the following form: given $\boldsymbol{\mu}_g \in \mathscr{P}_g$, find $\mathbf{d}_N(\boldsymbol{\mu}_g) \in \mathbb{R}^{N_d}$

$$\mathbb{B}_N(\boldsymbol{\mu}_g)\mathbf{d}_N(\boldsymbol{\mu}_g) = \mathbf{g}_N(\boldsymbol{\mu}_g), \tag{11}$$

and then, given $\boldsymbol{\mu}_p \in \mathscr{P}_p$, find $\mathbf{u}_N(\boldsymbol{\mu}) \in \mathbb{R}^{N_u}$ such that

$$\mathbb{A}_N(\boldsymbol{\mu})\mathbf{u}_N(\boldsymbol{\mu}) = \mathbf{f}_N(\boldsymbol{\mu}), \tag{12}$$

where the reduced matrices and vectors are given by

$$\mathbb{B}_N(\boldsymbol{\mu}_g) = \mathbb{V}^T\mathbb{B}(\boldsymbol{\mu}_g)\mathbb{V}, \qquad \mathbf{g}_N(\boldsymbol{\mu}_g) = \mathbb{V}^T\mathbf{g}(\boldsymbol{\mu}_g), \tag{13}$$

$$\mathbb{A}_N(\boldsymbol{\mu}) = \mathbb{W}^T\mathbb{A}(\mathbf{d}_N(\boldsymbol{\mu}_g);\boldsymbol{\mu}_p)\mathbb{W}, \qquad \mathbf{f}_N(\boldsymbol{\mu}) = \mathbb{W}^T\mathbf{f}(\mathbf{d}_N(\boldsymbol{\mu}_g);\boldsymbol{\mu}_p). \tag{14}$$

Here, we rely on the proper orthogonal decomposition (POD) method for the construction of the RB spaces. Once a set of snapshots of problems (6) and (10) has been computed, the singular value decomposition of the corresponding correlation matrices automatically yield optimal sets of orthonormal basis functions; see, e.g., [25] for further details. Note that each snapshot of problem (10) is computed on a different spatial domain, depending on the value of $\boldsymbol{\mu}_g$; nevertheless, this is not a concern, since we have assumed that the mesh deformation induced by $\mathbf{d}_h(\boldsymbol{\mu}_g)$ (and, correspondingly, by $\mathbf{d}_N(\boldsymbol{\mu}_g)$) does not affect the mesh connectivity and, as a result, the connectivity graph of the matrix $\mathbb{A}(\boldsymbol{\mu})$, too. The resulting POD-Galerkin technique allows to obtain two problems (11) and (12) of very small dimension.

Assembling the reduced matrices and vectors as in (13)–(14) when $\boldsymbol{\mu} \in \mathscr{P}$ varies is still too expensive in order to achieve efficient offline construction and online evaluation of the RB problem. As already mentioned, if the system matrices (resp. vectors) can be expressed as an affine combination of constant matrices (resp. vectors) weighted by suitable parameter-dependent coefficients, each term of the weighted sums can be projected offline onto the RB space spanned by $\mathbb{W}$, $\mathbb{V}$, respectively. For instance, if we assume that the matrix $\mathbb{A}(\boldsymbol{\mu})$ admits an affine decomposition

$$\mathbb{A}(\boldsymbol{\mu}) = \sum_{q=1}^{M_A} \theta_q^A(\boldsymbol{\mu})\mathbb{A}_q, \tag{15}$$

then

$$\mathbb{A}_N(\boldsymbol{\mu}) = \mathbb{W}^T\mathbb{A}(\boldsymbol{\mu})\mathbb{W} = \sum_{q=1}^{M_A} \theta_q^A(\boldsymbol{\mu})\,\mathbb{W}^T\mathbb{A}_q\mathbb{W},$$

where $\theta_q^A : \mathscr{P} \mapsto \mathbb{R}$ and $\mathbb{A}_q \in \mathbb{R}^{N_h^u \times N_h^u}$ are given functions and matrices, respectively, for $q = 1,\dots,M_A$; a similar affine decomposition made by M_f terms is required for the vector $\mathbf{f}(\boldsymbol{\mu})$ as well. Since the reduced matrices $\mathbb{W}^T\mathbb{A}_q\mathbb{W} \in \mathbb{R}^{N_u \times N_u}$ can be precomputed and stored offline, the online construction of the RB arrays in (14) for a given $\boldsymbol{\mu}$ is fast and efficient as long as $M_A, M_f \ll N_h^u$; a similar conclusion clearly holds for the RB arrays in (13), too.

In order to recover the affine structure (15) in those cases where the operator $\mathbb{A}(\boldsymbol{\mu})$ is nonaffine (i.e., (15) is not readily available), we must introduce a further level of reduction, called *hyper-reduction*; we thus refer to the resulting ROM as hyper-ROM (HROM). Here, we rely on DEIM to approximate the vectors $\mathbf{f}(\boldsymbol{\mu})$ and $\mathbf{g}(\boldsymbol{\mu}_g)$, and its matrix variant MDEIM to approximate $\mathbb{A}(\boldsymbol{\mu})$ and $\mathbb{B}(\boldsymbol{\mu}_g)$. A schematic summary of the entire offline/online computational strategy is offered in Fig. 2.

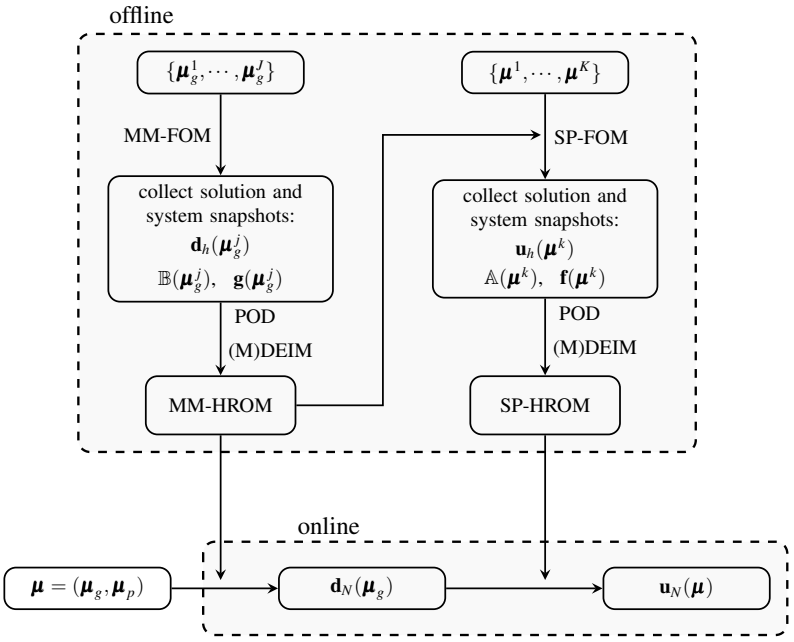

Fig. 2 Scheme of offline and online phases for the geometry and state reduction. Here MM-FOM and MM-HROM refer to (6) and (11), respectively (i.e. the full and hyper-reduced order models for the mesh motion (MM) problem). SP-FOM and SP-HROM refer instead to (10) and (12), respectively (i.e. the full and hyper-reduced order models for the state problem (SP))

3.3 Matrix DEIM

For the sake of space – and because of its relative novelty – here we only detail the way DEIM can be used to approximate a parameter-dependent matrix $\mathbb{K}(\tau)\colon \mathscr{T} \mapsto \mathbb{R}^{N_h \times N_h}$, where τ denotes a generic parameters vector. Given $\mathbb{K}(\tau)\colon \mathscr{T} \mapsto \mathbb{R}^{N_h \times N_h}$, the problem is to find $M \ll N_h$ functions $\theta_q\colon \mathscr{T} \mapsto \mathbb{R}$ and parameter-independent matrices $\mathbb{K}_q \in \mathbb{R}^{N_h \times N_h}$, $1 \leq q \leq M$, such that

$$\mathbb{K}(\tau) \approx \mathbb{K}_m(\tau) = \sum_{q=1}^{M} \theta_q(\tau)\, \mathbb{K}_q. \tag{16}$$

The offline stage of this procedure consists of two main steps. First we express $\mathbb{K}(\tau)$ in vector format by stacking its columns, that is, we set $\mathbf{k}(\tau) = \mathrm{vec}(\mathbb{K}(\tau)) \in \mathbb{R}^{N_h^2}$. Hence, (16) can be reformulated as: find $\{\boldsymbol{\Phi}, \boldsymbol{\theta}(\tau)\}$ such that

$$\mathbf{k}(\tau) \approx \mathbf{k}_m(\tau) = \boldsymbol{\Phi}\boldsymbol{\theta}(\tau), \tag{17}$$

where $\boldsymbol{\Phi} \in \mathbb{R}^{N_h^2 \times M}$ is a τ-independent basis and $\boldsymbol{\theta}(\tau) \in \mathbb{R}^M$ the corresponding coefficients vector. Then, we apply DEIM as in [6] to a set of snapshots $\boldsymbol{\Lambda} = [\mathrm{vec}(\mathbb{K}(\tau_1)), \ldots, \mathrm{vec}(\mathbb{K}(\tau_{n_s}))]$ in order to obtain the basis $\boldsymbol{\Phi}$ and a set of interpolation indices $\mathscr{I} \subset \{1, \cdots, N_h^2\}$. The former is computed by applying the POD technique over the columns of $\boldsymbol{\Lambda}$, whereas the latter is iteratively selected by employing the *magic points* algorithm [19].

During the online phase, given a new $\tau \in \mathscr{T}$, we can compute $\mathbb{K}_m(\tau)$ as

$$\mathbb{K}_m(\tau) = \mathrm{vec}^{-1}(\boldsymbol{\Phi}\boldsymbol{\theta}(\tau)) \qquad \text{with} \quad \boldsymbol{\theta}(\tau) = \boldsymbol{\Phi}_{\mathscr{I}}^{-1}\, \mathbb{K}_{\mathscr{I}}(\tau), \tag{18}$$

where $\boldsymbol{\Phi}_{\mathscr{I}}$ and $\mathbb{K}_{\mathscr{I}}(\tau)$ denote the matrices formed by the $\mathscr{I}$ rows of $\boldsymbol{\Phi}$ and $\mathbb{K}(\tau)$, respectively. We point out that, for the sake of model order reduction, the crucial step in the online evaluation of $\mathbb{K}_m(\tau)$ is the computation of $\mathbb{K}_{\mathscr{I}}(\tau)$. Nevertheless, this operation can be performed efficiently when $\mathbb{K}(\tau)$ results from a FE discretization of a PDE operator, by employing the same assembly routine used for the high-fidelity problem on the *reduced mesh* associated to the selected interpolation indices; see, e.g., [23] for further details.

4 Numerical example

As a proof of concept of the proposed technique, we consider a (direct) scattering problem dealing with the Helmholtz equation. Scattering problems are meant to study the effect that a bounded obstacle (or *scatterer*) has on incident waves, depending on the geometrical properties of the body; these latter are considered as geometrical parameters of interest. Such a problem is relevant in a wide range of applications such as the design of sonars and radars, medical imaging, geophysical exploration, and nondestructive testing [7]. Given the incident wave, the goal of a

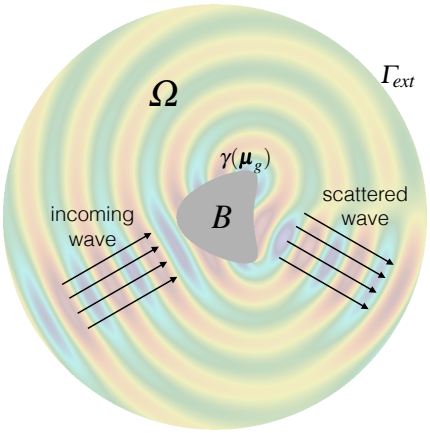

Fig. 3 Sketch of the domain and of the underlying physics; background coloring given by $\Re(u)$ for $\boldsymbol{\mu}_g = (-0.4, 1.2, 1.2)$, $\kappa = 5$, $a = \pi/6$.

direct scattering problem is to determine the scattered wave for the known obstacle; from a numerical standpoint, this is also a premise in view of the (indeed, very challenging) inverse scattering problem, in which the obstacle shape has to be reconstructed from far-field measurements. Helmholtz equations have already been tackled by RB methods, see, e.g. [28, 29, 17].

Let $B \subset \mathbb{R}^d$, $d = 2, 3$, the domain of an object with boundary $\gamma = \partial B$, and assume that $\gamma = \gamma(\boldsymbol{\mu}_g)$ is parametrized with respect to a vector of geometrical parameters $\boldsymbol{\mu}_g \in \mathscr{P}_g \subset \mathbb{R}^g$. The exterior domain is defined by the unbounded region $\mathscr{R} = \mathbb{R}^d \setminus B$; here we restrict ourselves to the case $d = 2$, although everything can be simply extended to the case $d = 3$ as well. Instead of considering an exterior acoustics problem in an unbounded domain, we truncate this latter by an artificial boundary Γ_{ext} where local absorbing boundary conditions are imposed; as a result, we deal with a bounded computational domain Ω, see Fig. 3.

Here we consider the propagation of time harmonic waves, for which the acoustic pressure P can be separated as $P(\mathbf{x}, t; \boldsymbol{\mu}) = \Re(u(\mathbf{x}; \boldsymbol{\mu}) e^{-i\omega t})$; the complex amplitude $u = u(\mathbf{x}; \boldsymbol{\mu})$ then satisfies the Helmholtz equation

$$\begin{aligned} \Delta u + \kappa^2 u &= 0 && \text{in } \Omega(\boldsymbol{\mu}_g) \\ u &= -e^{i\kappa \mathbf{a}\cdot\mathbf{x}} && \text{on } \gamma(\boldsymbol{\mu}_g) \\ \nabla u \cdot \mathbf{n} - i\kappa u &= 0 && \text{on } \Gamma_{ext}. \end{aligned} \tag{19}$$

Here $\kappa = \omega/c$ is the wave number, $\omega = 2\pi f$ the angular frequency and $c = 340$ cm s^{-1} the speed of sound. The scattered wave is time-harmonic, but not necessary plane, whereas the incident wave is considered to be a plane, time-harmonic wave $u^i(\mathbf{x}, t; \boldsymbol{\mu}) = e^{i(\kappa \mathbf{a}\cdot\mathbf{x} - \omega t)}$ with amplitude $A = 1$ and direction $\mathbf{a} = (\cos(a), \sin(a))^T$. On the boundary Γ_{ext} we prescribe a *first-order absorbing boundary condition*, yielding an approximation of the *Sommerfeld radiation condition*

$$\lim_{r\to\infty} r\left(\frac{\partial u}{\partial r} - iku\right) = 0$$

usually imposed in the case of unbounded domains [34]. In addition to the geometrical parameters $\boldsymbol{\mu}_g = (\alpha, \beta, \eta)$ encoding the shape of the obstacle B and the stiffening power, we also consider a vector of physical parameters $\boldsymbol{\mu}_p = (\kappa, a) \in \mathscr{P}_p \subset \mathbb{R}^p$ to model different scenarios where the wave number, as well as the direction, of the incident wave can vary.

We now apply the methodology developed in the previous sections to problem (19). The full-order model for the state Helmholtz problem is given by a $\mathbb{P}_1^{bubble}$ finite element approximation of (19), yielding a linear system of dimension $N_h^u = 147\,272$ obtained using a mesh made of 97934 triangular elements. Similarly, the full-order model for the mesh motion problem (1) is built using $\mathbb{P}_1^{bubble}$ finite elements, yielding a linear system of dimension $N_h^d = 294\,544$. Concerning the parameter range, we select $\alpha \in [-1/2, 1/2]$, $\beta \in [-0.81.2]$, $\eta \in [0, 1.4]$; instead, physical parameters range in $\kappa \in [2,5]$, $a \in [0, \pi/6]$.

We first consider the reduction of the mesh motion problem. We begin by computing a set of 50 solution, matrix and vector snapshots corresponding to 50 parameter samples selected by Latin Hypercube Sampling (LHS) design in $\mathscr{P}_g$. The eigenvalues of the correlation matrices of matrix and vector snapshots are reported in Fig. 4. Based on their decay, we retain the first $M_B = 5$ and $M_g = 11$ terms and then perform MDEIM and DEIM, respectively, to select the sets of interpolation indices. The reduced basis $\mathbb{V}$ is instead obtained by extracting $N = 10$ POD modes. In all these cases, a tolerance of $\varepsilon_{POD} = 10^{-5}$ has been imposed on the relative information content criterion, see [25]. Very few basis functions are then required to build an accurate ROM for the mesh motion problem, as it is shown by the convergence analysis reported in Fig. 5, left. The magnitude of the resulting RB displacement $\mathbf{d}_N(\boldsymbol{\mu})$) is instead reported in Fig. 5, right, for different parameter values.

Then, we turn to the reduction of the Helmholtz state problem – where $\Omega(\boldsymbol{\mu}_g)$ is approximated by $\Omega_h^N(\boldsymbol{\mu}_g)$, see equation (7) – following the same procedure as

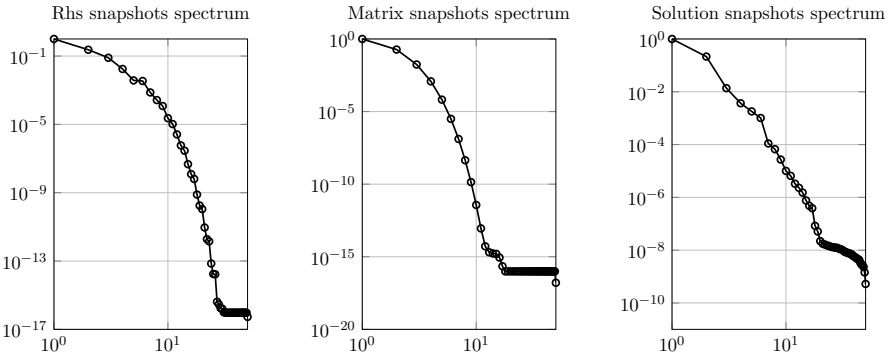

Fig. 4 Decay of the singular values of system and solution snapshots for the mesh motion problem

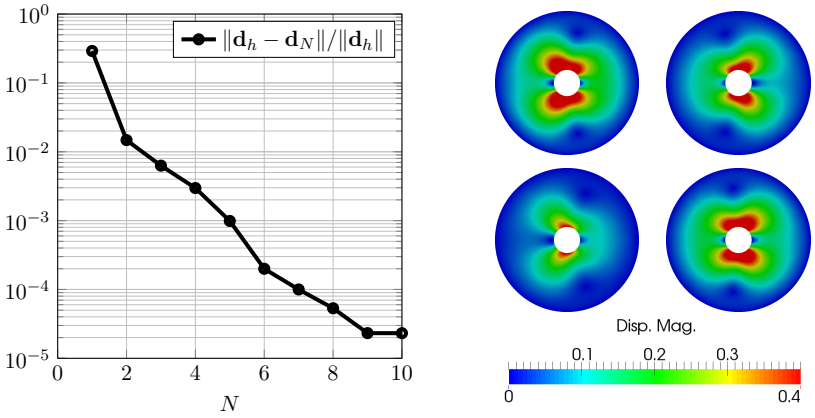

Fig. 5 Left: Relative error on the solution of the mesh motion problem (averaged over a test sample of 100 parameter values). Right: magnitude of the displacement $\mathbf{d}_N(\boldsymbol{\mu})$ for different parameter values

above. Regarding the system approximation, in this case $M_A = 60$ and $M_f = 142$ terms are selected out of 400 matrix and vector snapshots; concerning state reduction, we retain $N = 120$ basis functions, see Fig. 6.

Note that the decay of the eigenvalues of the correlation matrix is much slower than in the previous case highlighting a stronger variability of $\mathbf{u}_h(\boldsymbol{\mu})$ – as well as of the problem arrays $\mathbb{A}(\boldsymbol{\mu})$, $\mathbf{f}(\boldsymbol{\mu})$ – with respect to combined variations of both geometrical and physical parameters. This also translates into a much slower error convergence with respect to the RB dimension N_u, see Fig. 7, right. The resulting reduced mesh (see Fig. 7, left) is made of 291 elements, corresponding to about the 0.3% of the original ones; note that they concentrate around the obstacle, i.e. in the region where problem sensitivity to shape variations is higher. Some instances of the solution $u_N(\boldsymbol{\mu})$ to the Helmholtz equation obtained with the proposed technique are finally shown in Fig. 8; as a concluding remark, we point out that the online

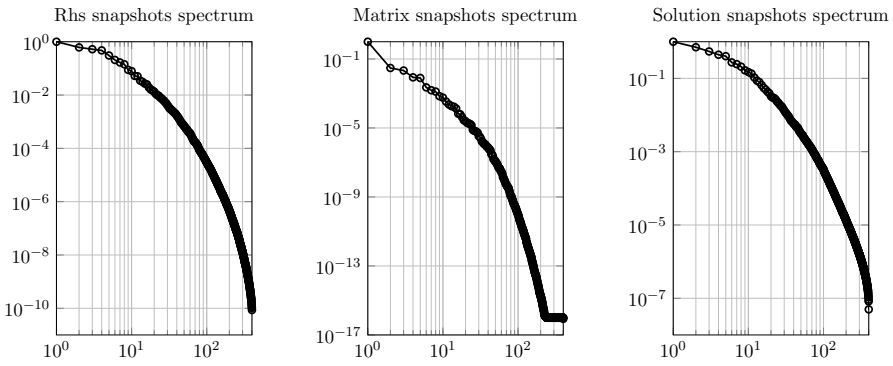

Fig. 6 Decay of the singular values of system and solution snapshots for the Helmholtz problem

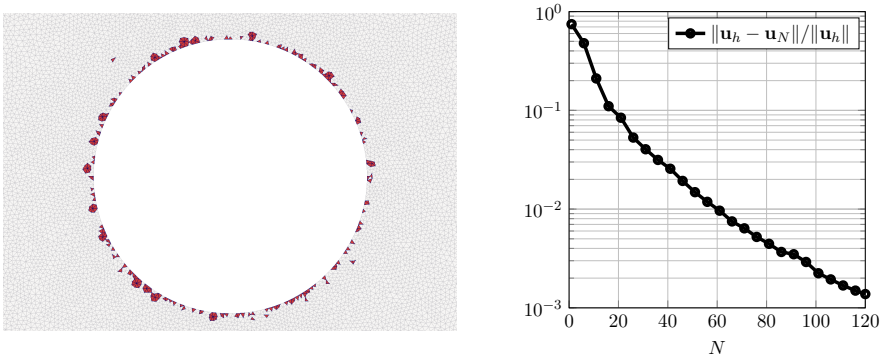

Fig. 7 Left: zoom of the reduced mesh (red elements) around the object. Right: relative error on the solution of the Helmholtz problem (averaged over a testing set of 200 parameter values)

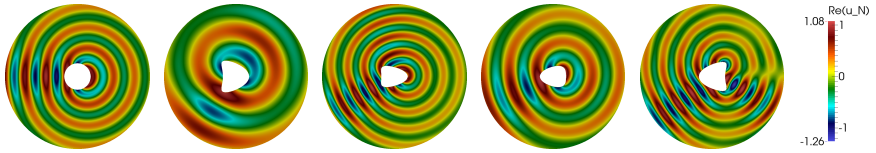

Fig. 8 $\Re(u_N(\boldsymbol{\mu}))$ for different values of the parameters

solution of both the reduced mesh motion (11) and the reduced Helmholtz problem (12) problems takes about $0.26s$, thus realizing a computational speedup of about 25 times with respect to the finite element FOM.

5 Conclusions

In this work we have presented a general and automatic way to deal with the efficient solution of parameterized PDEs defined on domains with variable shape. This framework combines a mesh motion technique relying on the solution of a solid extension problem, a POD-Galerkin reduced basis method, and a further hyper-reduction stage based on DEIM/MDEIM techniques. Compared to already existing strategies for handling mesh deformations in the RB context, the technique exploited in this work allows to directly define global domain deformations starting from boundary parametrizations. Indeed, relying on boundary – rather than volume – parametrizations is the most common and intuitive way to handle shape variations when design optimization is performed.

Although the proposed framework has been tested on a simplified case, where a single explicit boundary parametrization has been considered, its capabilities look promising in view of tackling a wider range of problems. For instance, it allows to handle different types of parametrizations simultaneously, each one defined on a separate portion of the boundary. Furthermore, it also applies in the case where a

database of boundary deformations results from the solution of a different problem – rather than from an explicit formula. This is the case, e.g., of fluid-structure interaction problems, where the deformation of the fluid-structure interface is an unknown of the problem itself; further work is ongoing in this respect.

References

1. Baker, T.: Mesh movement and metamorphosis. Engrg. Comput. **18**(3), 188–198 (2002)
2. Ballarin, F., Manzoni, A., Rozza, G., Salsa, S.: Shape optimization by free-form deformation: existence results and numerical solution for Stokes flows. J. Sci. Comput. **60**(3), 537–563 (2014)
3. Barrault, M., Maday, Y., Nguyen, N.C., Patera, A.T.: An 'empirical interpolation' method: application to efficient reduced-basis discretization of partial differential equations. C. R. Math. Acad. Sci. Paris **339**(9), 667–672 (2004)
4. Canuto, C., Tonn, T., Urban, K.: A posteriori error analysis of the reduced basis method for non-affine parameterized nonlinear PDEs. SIAM J. Numer. Anal. **47**(3), 2001–2022 (2009)
5. Carlberg, K., Tuminaro, R., Boggs, P.: Preserving Lagrangian structure in nonlinear model reduction with application to structural dynamics. SIAM J. Sci. Comput. **37**(2), B153–B184 (2015)
6. Chaturantabut, S., Sorensen, D.C.: Nonlinear model reduction via discrete empirical interpolation. SIAM J. Sci. Comput. **32**(5), 2737–2764 (2010)
7. Colton, D., Kress, R.: Inverse Acoustic and Electromagnetic Scattering Theory. Springer-Verlag, Berlin (2012)
8. Deparis, S., Forti, D., Quarteroni, A.: A rescaled localized radial basis function interpolation on non-cartesian and nonconforming grids. SIAM J. Sci. Comput. **36**(6), A2745–A2762 (2014)
9. Deparis, S., Løvgren, A.E.: Stabilized reduced basis approximation of incompressible three-dimensional Navier-Stokes equations in parametrized deformed domains. J. Sci. Comput. **50**(1), 198–212 (2012)
10. Forti, D., Rozza, G.: Efficient geometrical parametrisation techniques of interfaces for reduced-order modelling: application to fluid-structure interaction coupling problems. Int. J. Comput. Fluid. Dyn. **28**(3–4), 158–169 (2014)
11. Gordon, W., Hall, C.: Construction of curvilinear co-ordinate systems and applications to mesh generation. Int. J. Numer. Methods Engrg. **7**(4), 461–477 (1973)
12. Grepl, M.A., Maday, Y., Nguyen, N.C., Patera, A.T.: Efficient reduced-basis treatment of non-affine and nonlinear partial differential equations. ESAIM Math. Modelling Numer. Anal. **41**(3), 575–605 (2007)
13. Helenbrook, B.: Mesh deformation using the biharmonic operator. Int. J. Numer. Methods Engrg. **56**(7), 1007–1021 (2003)
14. Hesthaven, J., Rozza, G., Stamm, B.: Certified Reduced Basis Methods for Parametrized Partial Differential Equations. SpringerBriefs in Mathematics. Springer (2016)
15. Iapichino, L., Quarteroni, A., Rozza, G.: A reduced basis hybrid method for the coupling of parametrized domains represented by fluidic networks. Comput. Methods Appl. Mech. Engrg. **221–222**, 63–82 (2012)
16. Jäggli, C., Iapichino, L., Rozza, G.: An improvement on geometrical parameterizations by transfinite maps. C. R. Acad. Sci. Paris. Sér. I **352**(3), 263–268 (2014)
17. Lassila, T., Manzoni, A., Rozza, G.: On the approximation of stability factors for general parametrized partial differential equations with a two-level affine decomposition. ESAIM Math. Modelling Numer. Anal. **46**(6), 1555–1576 (2012)
18. Lassila, T., Rozza, G.: Parametric free-form shape design with PDE models and reduced basis method. Comput. Methods Appl. Mech. Engrg. **199**(23–24), 1583–1592 (2010)

19. Maday, Y., Nguyen, N.C., Patera, A.T., Pau, G.S.H.: A general multipurpose interpolation procedure: the magic points. Commun. Pure Appl. Anal. **8**(1), 383–404 (2009)
20. Manzoni, A., Quarteroni, A., Rozza, G.: Model reduction techniques for fast blood flow simulation in parametrized geometries. Int. J. Numer. Methods Biomed. Engng. **28(6–7)**, 604–625 (2012)
21. Manzoni, A., Quarteroni, A., Rozza, G.: Shape optimization of cardiovascular geometries by reduced basis methods and free-form deformation techniques. Int. J. Numer. Methods Fluids **70**(5), 646–670 (2012)
22. Manzoni, A., Salmoiraghi, F., Heltai, L.: Reduced basis isogeometric methods (RB-IGA) for the real-time simulation of potential flows about parametrized NACA airfoils. Comput. Meth. Appl. Mech. Engrg. **284**, 1147 – 1180 (2015)
23. Negri, F., Manzoni, A., Amsallem, D.: Efficient model reduction of parametrized systems by matrix discrete empirical interpolation. J. Comp. Phys. **303**, 431–454 (2015)
24. Nguyen, N.C.: A posteriori error estimation and basis adaptivity for reduced-basis approximation of nonaffine-parametrized linear elliptic partial differential equations. J. Comp. Phys. **227**, 983–1006 (2007)
25. Quarteroni, A., Manzoni, A., Negri, F.: Reduced Basis Methods for Partial Differential Equations. An Introduction, *Unitext*, vol. 92. Springer (2016)
26. Rozza, G., Huynh, D.B.P., Patera, A.T.: Reduced basis approximation and a posteriori error estimation for affinely parametrized elliptic coercive partial differential equations. Arch. Comput. Methods Engrg. **15**, 229–275 (2008)
27. Rozza, G., Lassila, T., Manzoni, A.: Reduced basis approximation for shape optimization in thermal flows with a parametrized polynomial geometric map. In: J.S. Hesthaven, E. Rønquist (eds.) Spectral and High Order Methods for Partial Differential Equations. Selected papers from the ICOSAHOM '09 conference, June 22-26, Trondheim, Norway, *Lecture Notes in Computational Science and Engineering*, vol. 76, pp. 307–315. Springer, Berlin Heidelberg (2011)
28. Sen, S.: Reduced basis approximation and a posteriori error estimation for non-coercive elliptic problems: application to acoustics. Ph.D. thesis, Massachusetts Institute of Technology (2007)
29. Sen, S., Veroy, K., Huynh, D.B.P., Deparis, S., Nguyen, N.C., Patera, A.T.: "Natural norm" a posteriori error estimators for reduced basis approximations. J. Comp. Phys. **217**(1), 37–62 (2006)
30. Staten, M., Owen, S., Shontz, S., Salinger, A., Coffey, T.: A comparison of mesh morphing methods for 3D shape optimization. In: Proceedings of the 20th international meshing roundtable, pp. 293–311. Springer (2011)
31. Stein, K., Tezduyar, T., Benney, R.: Mesh moving techniques for fluid-structure interactions with large displacements. J. Appl. Mech. **70**(1), 58–63 (2003)
32. Stein, K., Tezduyar, T., Benney, R.: Automatic mesh update with the solid-extension mesh moving technique. Comput. Meth. Appl. Mech. Engrg. **193**(21), 2019–2032 (2004)
33. Tezduyar, T., Behr, M., Mittal, S., Johnson, A.: Computation of unsteady incompressible flows with the stabilized finite element methods: Space-time formulations, iterative strategies and massively parallel implementations. In: New methods in transient analysis, vol. 246/AMD, pp. 7–24. ASME, New York (1992)
34. Thompson, L.: A review of finite-element methods for time-harmonic acoustics. J. Acoust. Soc. Am. **119**(3), 1315–1330 (2006)
35. Wirtz, D., Sorensen, D.C., Haasdonk, B.: A Posteriori Error Estimation for DEIM Reduced Nonlinear Dynamical Systems. SIAM J. Sci. Comput. **36**(2), A311–A338 (2014)
36. Zahr, M.J., Farhat, C.: Progressive construction of a parametric reduced-order model for PDE-constrained optimization. Int. J. Numer. Methods Engng. **102**(5), 1111–1135 (2015)

Recent publications:

MATHEMATICS INSTITUTE OF COMPUTATIONAL SCIENCE AND ENGINEERING
Section of Mathematics

Ecole Polytechnique Fédérale (EPFL)

CH-1015 Lausanne

07.2016 M. LANGE, S. PALAMARA, T. LASSILA, C. VERGARA, A. QUARTERONI, A.F. FRANGI:
Improved hybrid/GPU algorithm for solving cardiac electrophysiology problems on Purkinje networks

08.2016 ALFIO QUARTERONI, ALESSANDRO VENEZIANI, CHRISTIAN VERGARA:
Geometric multiscale modeling of the cardiovascular system, between theory and practice

09.2016 ROCCO M. LANCELLOTTI, CHRISTIAN VERGARA, LORENZO VALDETTARO, SANJEEB BOSE, ALFIO QUARTERONI:
Large Eddy simulations for blood fluid-dynamics in real stenotic carotids

10.2016 PAOLO PACCIARINI, PAOLA GERVASIO, ALFIO QUARTERONI:
Spectral based discontinuous Galerkin reduced basis element method for parametrized Stokes problems

11.2016 ANDREA BARTEZZAGHI, LUCA DEDÈ, ALFIO QUARTERONI:
Isogeometric analysis of geometric partial differential equations

12.2016 ERNA BEGOVIĆ KOVAČ, DANIEL KRESSNER:
Structure-preserving low multilinear rank approximation of antisymmetric tensors

13.2016 DIANE GUIGNARD, FABIO NOBILE, MARCO PICASSO:
A posteriori error estimation for the steady Navier-Stokes equations in random *domains*

14.2016 MATTHIAS BOLTEN, KARSTEN KAHL, DANIEL KRESSNER, FRANCISCO MACEDO, SONJA SOKOLOVIĆ:
Multigrid methods combined with low-rank approximation for tensor structured Markov chains

15.2016 NICOLA GUGLIELMI, MUTTI-UR REHMAN, DANIEL KRESSNER:
A novel iterative method to approximate structured singular values

16.2016 YVON MADAY, ANDREA MANZONI, ALFIO QUARTERONI :
An online intrinsic stabilitzation strategy for the reduced basis approximation of parametrized advection-dominated

17.2016 ANDREA MANZONI, LUCA PONTI :
An adjoint-based method for the numerical approximation of shape optimization problems in presence of fluid-structure interaction

18.2016 STEFANO PAGANI, ANDREA MANZONI, ALFIO QUARTERONI:
A reduced basis ensemble Kalman filter for state/parameter identification in large-scale nonlinear dynamical systems

19.2016 ANDREA MANZONI, FEDERICO NEGRI :
Automatic reduction of PDEs defined on domains with variable shape